

Intrinsic V vacancy and large magnetoresistance in $V_{1-\delta}Sb_2$ single crystal

Yong Zhang(张勇), Xinliang Huang(黄新亮), Jinglei Zhang(张警蕾), Wenshuai Gao(高文帅), Xiangde Zhu(朱相德), and Li Pi(皮雳)

Citation: Chin. Phys. B, 2022, 31 (**3**): 037102. DOI: 10.1088/1674-1056/ac3070
Journal homepage: http://cpb.iphy.ac.cn; http://iopscience.iop.org/cpb

What follows is a list of articles you may be interested in

Stability, electronic structure, and optical properties of lead-free perovskite monolayer $Cs_3B_2X_9$ (*B*=Sb, Bi; *X*=Cl, Br, I) and bilayer vertical heterostructure $Cs_3B_2X_9/Cs_3B_2'X_9$ (*B*,*B*'=Sb, Bi; *X*=Cl, Br, I)

Yaowen Long(龙耀文), Hong Zhang(张红), and Xinlu Cheng(程新路)
Chin. Phys. B, 2022, 31 (**2**): 027102. DOI: 10.1088/1674-1056/ac2e5f

Electronic and optical properties of 3N-doped graphdiyne/MoS_2 heterostructures tuned by biaxial strain and external electric field

Dong Wei(魏东), Yi Li(李依), Zhen Feng(冯振), Gaofu Guo(郭高甫), Yaqiang Ma(马亚强), Heng Yu(余恒), Qingqing Luo(骆晴晴), Yanan Tang(唐亚楠), and Xianqi Dai(戴宪起)
Chin. Phys. B, 2021, 30 (**11**): 117103. DOI: 10.1088/1674-1056/ac1927

Passivation and dissociation of P_b-type defects at a-SiO_2/Si interface

Xue-Hua Liu(刘雪华), Wei-Feng Xie(谢伟锋), Yang Liu(刘杨), and Xu Zuo(左旭)
Chin. Phys. B, 2021, 30 (**9**): 097101. DOI: 10.1088/1674-1056/ac0e20

Bilayer twisting as a mean to isolate connected flat bands in a kagome lattice through Wigner crystallization

Jing Wu(吴静), Yue-E Xie(谢月娥), Ming-Xing Chen(陈明星), Jia-Ren Yuan(袁加仁), Xiao-Hong Yan(颜晓红), Sheng-Bai Zhang(张绳百), and Yuan-Ping Chen(陈元平)
Chin. Phys. B, 2021, 30 (**7**): 077104. DOI: 10.1088/1674-1056/abd7d6

Tunable bandgaps and flat bands in twisted bilayer biphenylene carbon

Ya-Bin Ma(马亚斌), Tao Ouyang(欧阳滔), Yuan-Ping Chen(陈元平), and Yue-E Xie(谢月娥)
Chin. Phys. B, 2021, 30 (**7**): 077103. DOI: 10.1088/1674-1056/ac009e

---

Intrinsic V vacancy and large magnetoresistance in $V_{1-\delta}Sb_2$ single crystal

Yong Zhang(张勇)[1,2], Xinliang Huang(黄新亮)[2], Jinglei Zhang(张警蕾)[2], Wenshuai Gao(高文帅)[1,†], Xiangde Zhu(朱相德)[2,‡], and Li Pi(皮雳)[2]

[1] *Institutes of Physical Science and Information Technology, Anhui University, Hefei* 230601, *China*

[2] *Anhui Province Key Laboratory of Condensed Matter Physics at Extreme Conditions, High Magnetic Field Laboratory of the Chinese Academy of Sciences, Hefei* 230031, *China*

(Received 17 September 2021; revised manuscript received 8 October 2021; accepted manuscript online 18 October 2021)

The binary pnictide semimetals have attracted considerable attention due to their fantastic physical properties that include topological effects, negative magnetoresistance, Weyl fermions, and large non-saturation magnetoresistance. In this paper, we have successfully grown the high-quality $V_{1-\delta}Sb_2$ single crystals by Sb flux method and investigated their electronic transport properties. A large positive magnetoresistance that reaches 477% under a magnetic field of 12 T at $T = 1.8$ K was observed. Notably, the magnetoresistance showed a cusp-like feature at the low magnetic fields and such feature weakened gradually as the temperature increased, which indicated the presence of a weak antilocalization effect (WAL). In addition, based upon the experimental and theoretical band structure calculations, $V_{1-\delta}Sb_2$ is a research candidate for a flat band.

Keywords: binary pnictide semimetals, vanadium vacancy, flat band, weak anti-localization

PACS: 71.20.–b, 72.10.Fk, 72.15.Rn, 72.15.–v **DOI:** 10.1088/1674-1056/ac3070

1. Introduction

Topological insulators have attracted significant attention as they possess helical surface states protected by time reversal symmetry.[1–5] Due to the topological origin and Dirac fermion nature of the topological surface states, the topological insulators are expected to perform excellently in transport behaviors.[6,7] After the discovery of fascinating topological insulators, the binary pnictide semimetals XPm_2 (X = V, Nb, Ta; Pm = As, Sb)[8] (listed in Table 1) have also become a focus of attention in the field of condensed matter physics. The electronic structures of such materials are protected by an interplay of symmetry and topology. Electronic transport shows many novel quantum phenomena such as large non-saturation magnetoresistance (*MR*),[9–15] ultrahigh carrier mobility,[16] negative *MR*.[17–19] These multifunctional characteristics not only provide us a promising platform for fundamental physical research but also open up a new route for exploring the potential spintronic applications which is one of the most important reasons why these materials have stimulated unprecedented research.[20]

Table 1. Property of binary pnictide semimetals XPm_2.

Compound	Space group	Lattice parameters	Property	Reference
$NbAs_2$	$C12/m1$	$a = 9.368$ Å $b = 3.396$ Å $c = 7.799$ Å	Topological semimetal; non-saturating large *MR* (2000%, 9 T); negative longitudinal *MR*.	[19,23]
$NbSb_2$	$C12/m1$	$a = 10.239(1)$ Å $b = 3.630(1)$ Å $c = 8.3285(2)$ Å	Topological semimetal; anisotropic giant *MR* (1200%, 9 T); high mobilities.	[31]
TaP_2	$C12/m1$	$a = 6.88(16)$ Å $b = 3.2688(5)$ Å $c = 7.4992(14)$ Å	Weak topological insulator; negative longitudinal *MR*.	[10]
$TaAs_2$	$C12/m1$	$a = 9.370$ Å $b = 3.394$ Å $c = 7.771$ Å	Topological semimetal; negative longitudinal *MR* (10^6%, 9 T); high mobilities.	[13,14,17]
$TaSb_2$	$C12/m1$	$a = 10.222(4)$ Å $b = 3.645(2)$ Å $c = 8.292(3)$ Å	Anisotropic magnetoresistivity; ultrahigh carrier mobility; negative longitudinal *MR*.	[9,18]
VAs_2	$C12/m1$	$a = 9.05$ Å $b = 3.27$ Å $c = 7.46$ Å	Nodal-line semimetal; Kondo effect.	[16]
VSb_2	$I4/mcm$	$a = 6.5538$ Å $b = 6.5538$ Å $c = 5.6366$ Å	Large magnetoresistance (447%, 12 T); WAL.	[27] and our work.

†Corresponding author. E-mail: gwsh@ahu.edu.cn

‡Corresponding author. E-mail: xdzhu@hmfl.ac.cn

© 2022 Chinese Physical Society and IOP Publishing Ltd

VSb_2 has long been known as a thermoelectric material.[21] It has been recognized that this type of material is one of the candidates for diffusion barriers or electrodes in thermoelectric devices based on skutterudites.[22] Interestingly, VSb_2 crystallizes in tetragonal crystal structure, rather than the monoclinic one for other binary pnictides VAs_2,[16] $NbAs_2$,[19,23] and $TaAs_2$.[13] So far, there are a few researches on VSb_2 single crystal.[21] In this work, we successfully grow the large size and high-quality single crystals of $V_{1-\delta}Sb_2$. We systematically characterize its crystal structure, electrical transport, magnetism properties, specific heat, and calculated its band structure.

2. Experimental details

The high-quality $V_{1-\delta}Sb_2$ single crystals were synthesized by self-flux method.[24] V dendritic crystals (4N) and Sb (4N) pieces with V:Sb molar ratio of 1:30 were mixed and held in an alumina crucible, and sealed in an evacuated quartz tube. The quartz tube was heated to 1100 °C in 10 hours. After holding at this temperature for 20 hours, the tube was slowly cooled to 700 °C at a rate of 3 °C/h. The tube was then removed from the furnace and inverted into a centrifuge to remove the excess molten antimony. The resulting metallic luster single crystals with several millimeters size were collected from the crucible. The typical dimensions of the $V_{1-\delta}Sb_2$ single crystals are 1 mm×1 mm×0.5 mm and show no signs of instability or degradation when exposed to air. The compositions and elemental stoichiometry of the crystals were determined by energy-dispersive spectrometer (EDS) on Oxford X-MAX electron spectrometer equipped on the focused SEM/FIB dual beam system (Helios Nanolab600i, FEI Inc.).

A single crystal was selected and data were collected on a Bruker D8 Quest diffractometer with a detector using a Cu $K\alpha$ radiation source ($\lambda = 1.54184$ Å) from a rotating anode in a range of 10°–90°. Magnetization data were obtained from a Quantum Design magnetic property measurement system (MPMS-7) magnetometer with a 7-T superconducting magnet. The magnetization measurements of $V_{1-\delta}Sb_2$ single crystal were performed with zero-field cooling (ZFC) process on MPMS.

Electrode was made by spot welding using 25-μm gold wire, and electrical transport measurements were carried out by the four-probe method upon a physical property measurement system (Quantum Design, PPMS-14T) at a temperature range from 1.8 K to 300 K. During the measurements, a model 372 (AC) resistance bridge and temperature controller were used for the measurement of resistance with applied current of 3.16 mA. The low-temperature specific heat measurements were carried out upon a 16-T physical properties measurement system (Quantum Design, PPMS-16T) using the standard thermal relaxation method.

The preliminary first-principles band structure calculations were performed based on the density functional theory (DFT), and use the projector augmented wave method as implemented in the Vienna *ab initio* simulations package (VASP).[25] The generalized gradient approximation with the Perdew–Burke–Ernzerhof (PBE)[26] realization was adopted for the exchange–correlation functional. The cutoff energy was set as 400 eV. The energy and force convergence criteria were set to be 10^6 eV and -0.05 eV/Å, respectively.

3. Results and discussion

According to the previous report,[27] $CuAl_2$-type structure $V_{1-\delta}Sb_2$ crystallizes in the tetragonal $I4/mcm$ space group (No. #140). Figures 1(a) and (b) show the crystal structure of $V_{1-\delta}Sb_2$, which can be regarded as alternating stacking layers of V and Sb atoms by ABAB sequence along the c axis. Each V atom is octahedrally coordinated by Sb atoms with a bond distance of 2.484(8) Å.[28]

Figure 1(c) shows the EDS spectrum for $V_{1-\delta}Sb_2$, the measurements were performed at different positions on the polished surface of the crystal. The average chemical composition ratio of V:Sb was established to be 31.45%:68.55%, which confirms the existence of V atoms vacancies in the $V_{1-\delta}Sb_2$ single crystal with $\delta \approx 0.08$. This value is approximately in accordance with previous phase diagram studies ($V_{0.9}Sb_2$[29] and $V_{0.97}Sb_2$[21,22]). This means that $V_{1-\delta}Sb_2$ phase with V vacancy is more stable at ambient pressure, while VSb_2 with the same space group $C12/m1$ as $NbAs_2$ may be stabilized under high pressure.

Figure 1(d) shows the single crystal XRD pattern for the $V_{1-\delta}Sb_2$ at room temperature. Two sharp diffraction peaks that represent (00l) plane can be observed. The inset shows the rocking curve of the (002) diffraction peak, the full width at half-maximum (FWHM) is estimated to be $\Delta\theta \approx 0.05°$. Such a narrow FWHM indicates the high quality of the single crystal without twin crystal.

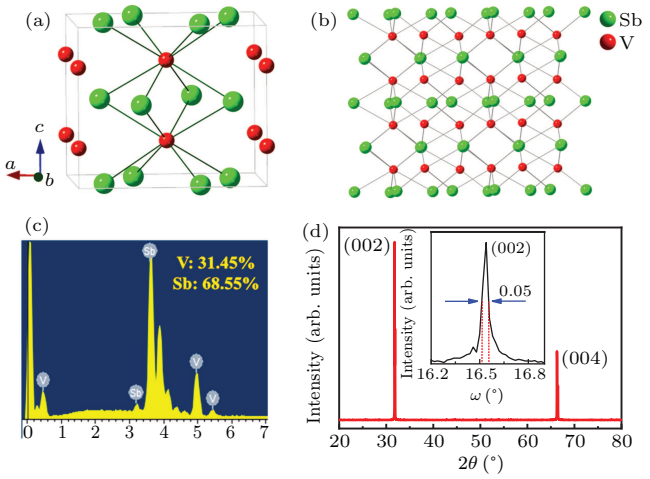


Fig. 1. (a) and (b) Crystal structure of the $V_{1-\delta}Sb_2$ single crystal. The red sphere represents vanadium atoms, the green sphere represents antimony atoms. (c) The topical energy dispersive spectrometer (EDS) for single crystal $V_{1-\delta}Sb_2$. (d) X-ray diffraction pattern of $V_{1-\delta}Sb_2$ single crystal with the corresponding Miller indices (00L) in parentheses. The inset shows a corresponding rocking curve.

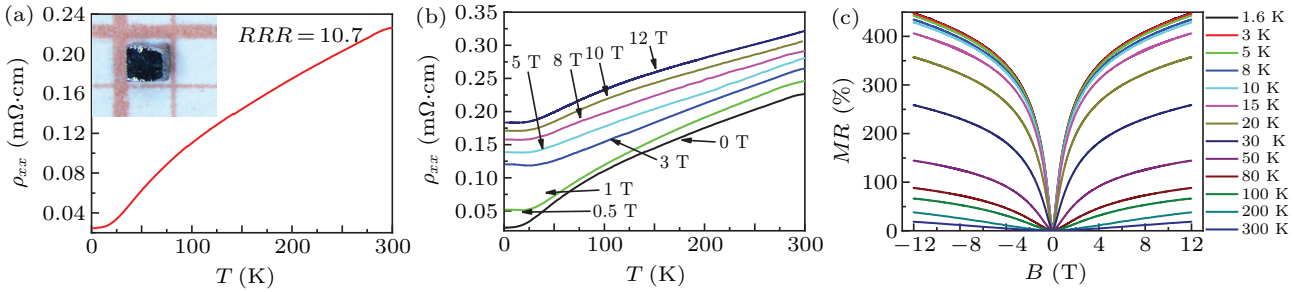


Fig. 2. (a) The temperature dependence of longitudinal ρ_{xx} from 1.8 K to 300 K at the zero magnetic field. The value of *RRR* is 10.7. Upper inset shows a photograph of $V_{1-\delta}Sb_2$ single crystal on millimeter-grid paper. (b) The ρ_{xx} at different magnetic fields. (c) The normalized *MR* at temperature ranging from 1.8 K to 300 K.

Figure 2(a) exhibits the temperature dependence of longitudinal resistivity ρ_{xx} for $V_{1-\delta}Sb_2$ single crystal in the temperature range of 300 K–1.8 K without magnetic field. The inset displays the typical view of a $V_{1-\delta}Sb_2$ single crystal placed on a millimeter grid with the preferential orientation along the [001] zone axis. The residual resistance ratio (*RRR*), $RRR = \rho_{xx}(300\ \mathrm{K})/\rho_{xx}(2\ \mathrm{K}) = 10.8$, is relatively lower than that of VAs_2(12),[16] $NbAs_2$(150),[23] and $NbSb_2$ (~ 200).[30] This value is still larger than the reported value of ~ 3.0 in Ref. [22]. Such relatively low value of *RRR* for $V_{1-\delta}Sb_2$ should origin from the intrinsic V vacancy, which provides additional scattering centers.

When the temperature decreases from 300 K to 1.8 K, the ρ_{xx} exhibits metallic behavior. Figure 2(b) plots the temperature dependence of resistivity under different magnetic fields. The electric current is parallel to the *b* axis, and the magnetic field is perpendicular to the *ab* plane. When a magnetic field is applied to the $V_{1-\delta}Sb_2$ single crystal, the ρ_{xx} curves are enhanced obviously with increased magnetic and another important fact observed is that $\rho_{xx}(T)$ also increases 18.2% at 12 T at room temperature (300 K). Moreover, the $V_{1-\delta}Sb_2$ still holds metallic behavior even at high field of 12 T without any sign of metal–insulator transition, which is quite different from the observation of insulator-like behavior in other binary pnictide semimetals.[12,13,30–32]

Figure 2(c) shows the normalized *MR* curves measured at different temperatures and the magnetic field is applied perpendicular to the (*001*) plane. The *MR* is defined as

$$MR = \frac{\rho_{xx}(H) - \rho_{xx}(0)}{\rho_{xx}(0)} \times 100\%.$$

Here $\rho_{xx}(H)$ and $\rho_{xx}(0)$ are longitudinal resistivities with and without magnetic field, respectively. The normalized *MR* curves are symmetrized via $MR(B) = [MR(B) + MR(-B)]/2$ to remove the contribution of Hall resistance. At $T = 1.8$ K, $V_{1-\delta}Sb_2$ single crystal exhibits a large *MR* of 447% at $B =$ 12 T. With the increase of temperature, *MR* is suppressed significantly but still remain about 18.2% at 300 K. The classical carrier compensation mechanism was used to explain the large and non-saturating quadratic *MR*, such as that of in WP_2[33] and Nb_3Sb.[34] Based on the band structure calculation in Fig. 5, although we observed the electron and hole pockets from Γ to X point, such a mechanism seemed to be invalid because the field dependence of *MR* in $V_{1-\delta}Sb_2$ single crystal was of significant deviation from quadratic behavior. On the other hand, similar large *MR* behavior had been observed in nonmagnetic half-Heusler ScPtBi single crystals.[35] Therefore, the large *MR* for $V_{1-\delta}Sb_2$ single crystal could be understood as the WAL effect makes resistance increase steeply near zero fields. Remarkably, we observed that the *MR* increases sharply in the low field region under 20 K, and a large *MR* of 180% is obtained in a magnetic field of 1 T at 1.8 K. The *MR* in $V_{1-\delta}Sb_2$ single crystal is much larger than many other nonmagnetic compounds, such as ScPdBi,[36] LuPtSb,[37] and Bi_2Te_3.[38] This distinct *MR* dip near zero magnetic field can be associated with the weak antilocalization (WAL) effect. The WAL effect is generally expected to originate from the topologically protected surface state,[39–41] or strong spin–orbit coupling.[42] At zero magnetic field, backscattering gains the minimum due to the time-reversal symmetry. As the magnetic field increases, the time-reversal symmetry is broken and the backscattering increases, which leads to a sharp increase of *MR*. It has been widely observed in topological insulators (Bi–Se–Te[43–45]) and topological superconductors (Al–InAs[46] and LuPdBi[47]). Furthermore, such phenomenon has also been reported in systems with strong spin–orbit couplings, such as LuPtSb[37] and YPdBi.[48]

In order to deeply understand the WAL effect in $V_{1-\delta}Sb_2$ single crystal, we fit the corresponding magnetoconductivity $\Delta\sigma_{xx}(B) = \sigma_{xx}(B) - \sigma_{xx}(0)$ using the Hikami–Larkin–Nagaoka (HLN) formula[49]

$$\Delta\sigma_{xx}(B) = \frac{\alpha e^2}{2\pi^2\hbar}\left[\psi\left(\frac{1}{2} + \frac{\hbar}{4eBL_\varphi}\right) - \ln\left(\frac{\hbar}{4eBL_\varphi}\right)\right], \quad (1)$$

where e and $\hbar$ are electron charge and reduced Planck constant; ψ is digamma function; α and L_φ are the prefactor and phase coherence length, respectively. The prefactor α denotes the number of conduction channels, which is experimentally found to be -0.5 for each conductive channel in two-dimensional (2D) topological insulator. Figure 3(a) displays the low-field magnetoconductivity $\Delta\sigma_{xx}(B)$ from -0.3 T to 0.3 T at temperatures ranging from 1.8 K to 20 K, and all the curves can be well fitted by the HLN model. The obtained phase coherence length L_φ as a function of temperature

are shown in Figure 3(b), and the inset displays the temperature dependence of parameters α. Remarkably, the value of α with an order of 10^5 is larger than the theoretical 2D electron system, hinting that the WAL effect is mainly originate from the strong spin–orbit coupling of the three-dimensional (3D) bulk state in the $V_{1-\delta}Sb_2$ single crystal. In addition, we measure the angle-dependent $\Delta\sigma_{xx}(B)$ at 1.8 K under low magnetic fields from −1 T to 1 T, as shown in Fig. 3(c). In the 2D topological insulator, the $\Delta\sigma_{xx}$ *versus* $B\sin\theta$ curves should converge to one curve. The $\Delta\sigma_{xx}$ *versus* $B\sin\theta$ curves in $V_{1-\delta}Sb_2$ are separate from each other, which further confirms the 3D feature of the WAL effect. All the results reveal that the WAL effect in $V_{1-\delta}Sb_2$ is resulted from strong spin–orbit coupling (SOC) destructive quantum interference between time-reversed loops formed by scattering trajectories, leading to the conductivity enhanced with decreasing temperature in the 3D bulk transport.[41]

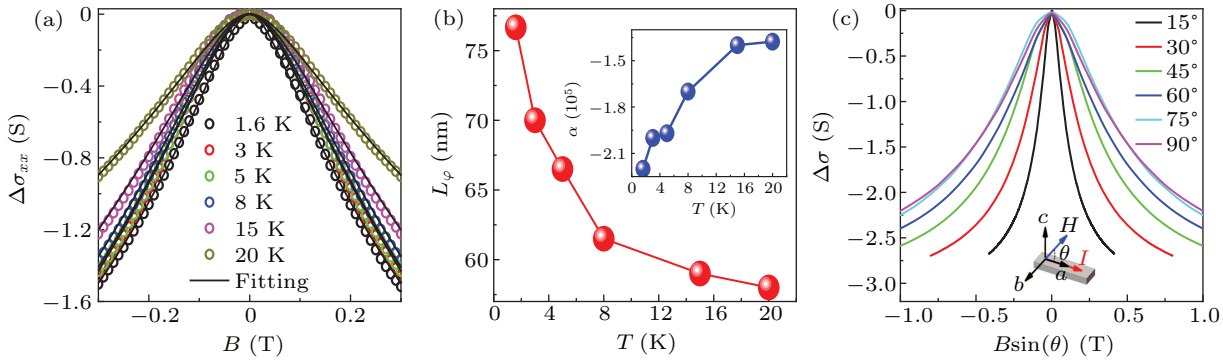


Fig. 3. (a) The normalized magnetoconductance ($\Delta\sigma_{xx}$) at different temperatures (color hollow circle) and the black line is corresponding fitting curve. (b) Temperature dependence of the fitting parameter L_φ phase coherence length deduced from the WAL fit. The inset shows the temperature dependence of α. (c) The $\Delta\sigma_{xx}$ plotted in the perpendicular magnetic field component of the magnetic field, $B\sin\theta$, at 1.8 K. Inset, schematic diagram of the measurement setup where θ indicates the angle between the direction of the magnetic field and (001) plane.

In addition, we measured the anisotropic magnetic properties of the $V_{1-\delta}Sb_2$ single crystal. Figure 4(a) shows the magnetic susceptibility χ–T curve with applied magnetic field parallel and perpendicular to (001) plane, respectively. Obviously, the temperature-dependent paramagnetic susceptibility curves show typical paramagnetic behavior with nonnegligible anisotropic, and the χ_c is relatively larger than χ_{ab}. Both curves can be well fitted with the Curie–Weiss law $\chi = \chi_0 + C/(T-\theta)$,[50] where χ_0 is the temperature-dependent paramagnetic susceptibility from the electron contribution near the Fermi level, C is Curie constant, θ is the Weiss temperature. For both curves, the determined C and θ are almost identical with the values of about 0.0174(9) emu·mol^{-1}·Oe^{-1}·K^{-1} (1 Oe = 79.5775 A/m) and −183.7(3) K, respectively. The effective momentum was determined to be 0.3741 μ_B/V atom. The negative θ value indicates the existence of antiferromagnetic coupling between V atoms or vacancy. By subtracting the Curie–Weiss part, the χ_0 part can be obtained and is shown in the inset of Fig. 4(a). Apparently, χ_0 for $H||c$ remains in whole temperature range down to 4 K with a small curie tail, while χ_0 for $H||ab$ starts to increase suddenly with decreasing temperature below 15 K. Such a sudden increase of χ_0 for $H||ab$ may not come from magnetic order, since the antiferromagnetic coupling. Figure 4(b) shows the typical paramagnetic behaviors for $H||c$, and the magnetization is extremely small at 2 K, which confirmed that an abrupt increase of the χ_0 part is not induced by the magnetic order. On the other hand, if we attribute the abrupt magnetization increment ΔM between 2 K and 20 K (3.4×10^{-2} emu·mol^{-1}) to the ferromagnetic impurity, we can obtain a concentration with 10^{-6} order for magnetic impurity. In classic condensed matter physics, the χ_0 is proportional to the density of Fermi level with small magnetic field H with relation of[51]

$$\chi = \frac{N\mu_0\mu_B^2}{k_B T_F}, \tag{2}$$

where N represents the density of states at the Fermi level, μ_0 is the magnetic permeability of free space, μ_B is the Bohr magneton, k_B is the Boltzmann's constant, and T_F is the Fermi temperature. Therefore, anisotropic increase of χ_0 suggests that the density of states N increase abruptly at low temperature. Since the electronic heat capacity part γ is proportional to $N^{1/3}$and effective mass m^* at low temperature with equation[52]

$$\gamma = \frac{m^*}{m}\frac{4\pi^3 m k_B^2}{3h^2}\left(\frac{3NV^2}{\pi}\right)^{1/3}, \tag{3}$$

where m is the mass of free electrons, h is the Planck constant, V is the volume per mole. Theoretically, an abrupt increase of N at low temperature is expected to yield an abrupt increase of γ in specific heat.

Heat capacity was measured between 2 K to 10 K and no phase transition was observed. The total heat capacity of normal metal material at low temperature can be described as the sum of $C = C_e + C_p = \gamma T + \beta T^3$,[52] where C_p is the phonon

contribution, γ and β are the free electron part coefficient and phonon part coefficient. To obtain the γ part, C/T *versus* T^2 curve is plotted in Fig. 4(c). By linear fitting of the curve, phonon part coefficient $\beta = 0.16529$ mJ·mol^{-1}·K^{-4} can be obtained. As shown in Fig. 4(c), the C/T–T^2 deviates from the simple model for a normal metal below 7 K. As mentioned above, the estimated low concentration of ferromagnetic impurity is of 10^{-6} order, which cannot explain the heat capacity change below 7 K. After subtracting the phonon part, the temperature dependence of γ can be obtained, as displayed in Fig. 4(d). We propose that the γ free electron part suddenly increases under 7 K, which means that the abrupt increase of γ induced by the abrupt increase of N at low temperature. To figure out the physics origin, band structure calculations were made.

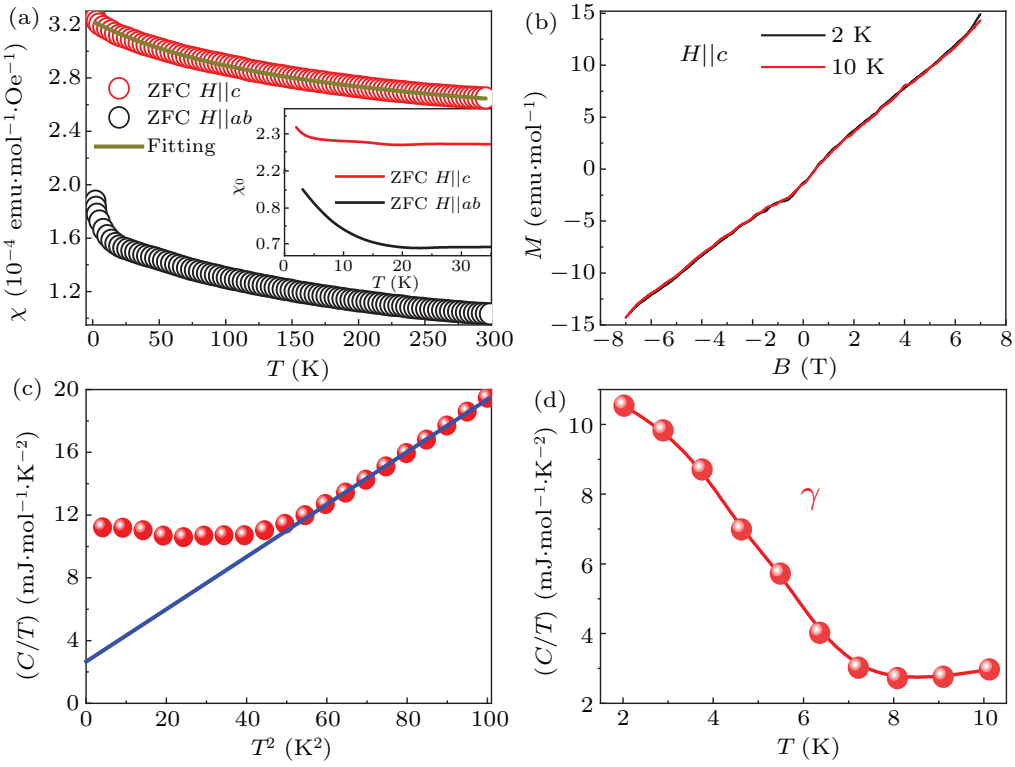


Fig. 4. (a) The magnetic susceptibility of $V_{1-\delta}Sb_2$ single crystal with under zero field cooling (ZFC) for field of 0.2 T applied parallel to c axis and perpendicular to ab plane. The brown line is fitting with the Curie–Weiss law and the inset shows a temperature-dependent paramagnetic susceptibility gained by magnetic susceptibility subtracted the Curie–Weiss part. (b) Field-dependent magnetization at 2 K, 10 K, respectively. (c) $C(T)/T$ *versus* T^2 of $V_{1-\delta}Sb_2$ single crystal from 2 K to 10 K. (d) The free electron part coefficient $\gamma(C/T–\beta T^2)$ *versus* temperature T, where β is determined from the linear fitting (blue solid line).

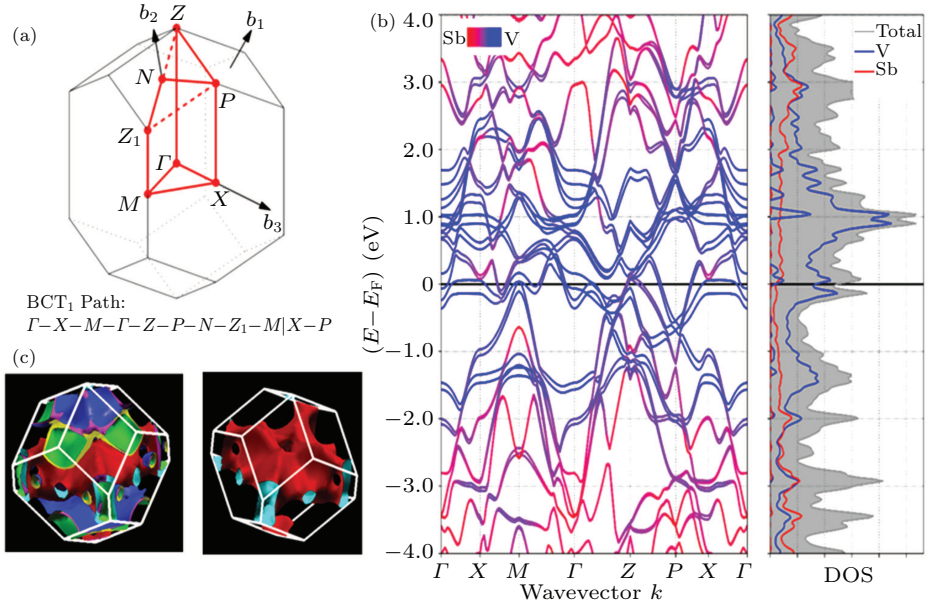


Fig. 5. (a) The Brillouin zones. (b) Band structures calculated with considering spin–orbit coupling (SOC) and the total density of states (DOS) for VSb_2. (c) The Fermi surfaces of VSb_2 crystals from first-principle calculations. Left is total Fermi surface for VSb_2, right is Fermi surface with along Γ–X.

We first calculated the band structures with SOC. The obtained results are plotted in Fig. 5(b). Then, the Fermi surface was calculated by the VASPKIT.[25] The software of XcrySDen was used to plot the Fermi surface in Fig. 5(c). Figure 5(a) shows the first Brillouin zone in momentum space for the primitive unit cell. The metallic character can be shown by the high density of states (DOS) at the Fermi level and the presence of electron and hole-bands. The DOS of VSb_2 shows that the region close to Fermi level is dominated by fully occupied V-3d states with a small contribution of Sb-3p states and that conduction bands are dominated strongly by this hybridization.[27] The left of Fig. 5(c) reveals the total Fermi surface include the six bands crossing Fermi level. The right picture shows a flat band, that crosses the Fermi surface along Γ–X point, consists of hole- and electron-pockets. The electron-pocket encompasses the Γ point. The hole-pockets, located on the X point, which is in the center of the hexagonal plane of Brillouin zone. According to the previous research, from 300 K to 10 K, $V_{0.97}Sb_2$ single crystal has a relatively large linear coefficient of thermal expansion $\alpha_l = 14.1 \times 10^{-6}$ K^{-1}, which value is higher than the reported value for $NbSb_2$ (8.4×10^{-6} K^{-1}) and $TaSb_2$ (7.5×10^{-6} K^{-1}).[22] With the decrease of temperature, the structure of $V_{1-\delta}Sb_2$ single crystal is distorted and the flat band gradually approached the Fermi surface. When the temperature falls below 7 K, the flat band is closer to the Fermi surface and produces a large density of states. This is the reason why the magnetic susceptibility and the C_e increase at low temperatures.

4. Conclusions

High-quality $V_{1-\delta}Sb_2$ single crystals were grown via flux method. Due to VSb_2 possesses a narrow homogeneity range, the vanadium compound possesses a V deficiency and is better described as $V_{1-\delta}Sb_2$ ($\delta \approx 0.08$). We have calculated the electronic structure with SOC and measured the longitudinal resistivity, specific heat, and magnetic susceptibility of $V_{1-\delta}Sb_2$. Transport experiments demonstrated that $V_{1-\delta}Sb_2$ performs metallic behavior with positive large *MR* reached 447%. More intriguingly, we observed an obvious WAL effect from *MR* below 20 K in the low-field region. The extremely large α and the angle dependence of $\Delta\sigma_{xx}$ suggest that the WAL effect in $V_{1-\delta}Sb_2$ single-crystal originates from the contribution of strong 3D bulk spin–orbital coupling. In addition, we observed the abruptly increase of the χ_0 part and C_e part under the 7 K. We propose that these phenomena are signatures of the flat band, which indicates $V_{1-\delta}Sb_2$ is likely to display fantastic electronic behaviors at extremely low temperatures.

Acknowledgements

Project supported by the National Natural Science Foundation of China (Grant Nos. U2032214, U2032163, and 11904002), the Youth Innovation Promotion Association of Chinese Academy of Sciences (Grant No. 2017483), and the Natural Science Foundation of Anhui Province, China (Grant No. 1908085QA15).

References

[1] Hasan M Z and Kane C L 2010 *Rev. Mod. Phys.* **82** 3045
[2] Qi X and Zhang S 2011 *Rev. Mod. Phys.* **83** 1057
[3] Ando Y 2013 *J. Phys. Soc. Jpn.* **82** 102001
[4] Ando Y and Fu L 2015 *Annu. Rev. Condens. Matter Phys.* **6** 361
[5] Moore J E 2010 *Nature* **464** 194
[6] Zhang T, Cheng P, Chen X, Jia J F, Ma X, He K, Wang L, Zhang H, Dai X, Fang Z, Xie X and and Xue Q K 2009 *Phys. Rev. Lett.* **103** 266803
[7] Roushan P, Seo J, Parker C V, Hor Y S, Hsieh D, Qian D, Richardella A, Hasan M Z, Cava R J and Yazdani A 2009 *Nature* **460** 1106
[8] Xu C, Chen J, Zhi G, Li Y, Dai J and Cao C 2016 *Phys. Rev. B* **93** 195106
[9] Liu X Y, Wang J L, You W, Wang T T, Yang H Y, Jiao W H, Mao H Y, Zhang L, Cheng J and Li Y K 2017 *Chin. Phys. Lett.* **34** 127501
[10] Wang H, Su H, Zhang J, Xia W, Lin Y, Liu X, Hou X, Yu Z, Yu N, Wang X, Zou Z, Wang Y, Liang Q, Zhen Y and Guo Y 2019 *Phys. Rev. B* **100** 115127
[11] Peramaiyan G, Sankar R, Muthuselvam I P and Lee W L 2018 *Sci. Rep.* **8** 6414
[12] Wang Y, Yu Q, Guo P, Liu K and Xia T 2016 *Phys. Rev. B* **94** 041103
[13] Yuan Z, Lu H, Liu Y, Wang J and Jia S 2016 *Phys. Rev. B* **93** 184405
[14] Wu D, Liao J, Yi W, Wang X, Li P, Weng H, Shi Y, Li Y, Luo J, Dai X and Fang Z 2016 *Appl. Phys. Lett.* **108** 042105
[15] Leahy I A, Lin Y P, Siegfried P E, Treglia A C, Song J C W, Nandkishore R M and Lee M 2018 *Proc. Natl. Acad. Sci. USA* **115** 10570
[16] Chen S, Lou Z, Zhou Y, Chen Q, Xu B, Wu C, Du J, Yang J, Wang H and Fang M 2021 *Chin. Phys. Lett.* **38** 017202
[17] Luo Y, McDonald R D, Rosa P F, Scott B, Wakeham N, Ghimire N J, Bauer E D, Thompson J D and Ronning F 2016 *Sci. Rep.* **6** 27294
[18] Li Y, Li L, Wang J, Wang T, Xu X, Xi C, Cao C and Dai J 2016 *Phys. Rev. B* **94** 121115
[19] Shen B, Deng X, Kotliar G and Ni N 2016 *Phys. Rev. B* **93** 195119
[20] Kumar N, Sun Y, Xu N, Manna K, Yao M, Suss V, Leermakers I, Young O, Forster T, Schmidt M, Borrmann H, Yan B, Zeitler U, Shi M, Felser C and Shekhar C 2017 *Nat. Commun.* **8** 1642
[21] Malki S and El Farh L 2020 *Int. J. Thermophys.* **41** 58
[22] Failamani F, Broz P, Macciò D, Puchegger S, Müller H, Salamakha L, Michor H, Grytsiv A, Saccone A, Bauer E, Giester G and Rogl P 2015 *Intermetallics* **65** 94
[23] Harimohan V, Bharathi A, Babu P D, Rajaraman R and Sundar C S 2020 *AIP Conf. Proc.* **2265** 030428
[24] Canfield P C 2020 *Rep. Prog. Phys.* **83** 016501
[25] Wang V, Xu N, Liu J C, Tang G and Geng W 2021 *Comput. Phys. Commun.* **267** 108033
[26] Perdew J P, Burke K and Ernzerhof M 1996 *Phys. Rev. Lett.* **77** 3865
[27] Malki S and EL Farh L 2019 *Materials Today-Proceedings* **13** 991
[28] Havinga E E, Damsma H and Hokkeling P 1972 *Journal of the Less Common Metals* **27** 169
[29] Armbrüster M, Schnelle W, Schwarz U and Grin Y 2007 *Inorg. Chem.* **46** 6319
[30] Wang K, Graf D, Li L, Wang L and Petrovic C 2014 *Sci. Rep.* **4** 7328
[31] Zhang C L, Yuan Z J, Jiang Q D, Tong B B, Zhang C, Xie X C and Jia S 2017 *Phys. Rev. B* **95** 085202
[32] Shekhar C, Nayak A K, Sun Y, Schmidt M, Nicklas M, Leermakers I, Zeitler U, Skourski Y, Wosnitza J, Liu Z K, Chen Y L, Schnelle W, Borrmann H, Grin Y, Felser C and Yan B H 2015 *Nat. Phys.* **11** 645
[33] Zhang K, Du Y, Wang P, Wei L, Li L, Zhang Q, Qin W, Lin Z, Cheng B, Wang Y, Xu H, Fan X, Sun Z, Wan X and Zeng C 2020 *Chin. Phys. Lett.* **37** 090301
[34] Chen Q, Zhou Y, Xu B, Lou Z, Chen H, Chen S, Wu C, Du J, Wang H, Yang J and Fang M 2021 *Chin. Phys. Lett.* **38** 087501

[35] Hou Z, Wang Y, Liu E, Zhang H, Wang W and Wu G 2015 *Appl. Phys. Lett.* **107** 202103

[36] Zhang J, Hou Z, Zhang C, Chen J, Li P, Wen Y, Zhang Q, Wang W and Zhang X 2019 *Appl. Phys. Lett.* **115** 172407

[37] Hou Z, Wang Y, Xu G, Zhang X, Liu E, Wang W, Liu Z, Xi X, Wang W and Wu G 2015 *Appl. Phys. Lett.* **106** 102102

[38] Wang X, Du Y, Dou S and Zhang C 2012 *Phys. Rev. Lett.* **108** 266806

[39] Chen J, Qin H J, Yang F, Liu J, Guan T, Qu F M, Zhang G H, Shi J R, Xie X C, Yang C L, Wu K H, Li Y Q and Lu L 2010 *Phys. Rev. Lett.* **105** 176602

[40] Lu H Z and Shen S 2011 *Phys. Rev. B* **84** 125138

[41] Liu W E, Hankiewicz E M and Culcer D 2017 *Materials* **10** 807

[42] Bergmann G 1984 *Phys. Rep.* **107** 1

[43] Kim Y S, Brahlek M, Bansal N, Edrey E, Kapilevich G A, Iida K, Tanimura M, Horibe Y, Cheong S W and Oh S 2011 *Phys. Rev. B* **84** 073109

[44] Shrestha K, Graf D, Marinova V, Lorenz B and Chu C W 2017 *J. Appl. Phys.* **122** 145901

[45] He H, Wang G, Zhang T, Sou I K, Wong G K L, Wang J, Lu H, Shen S and Zhang F 2011 *Phys. Rev. Lett.* **106** 166805

[46] Das A, Ronen Y, Most Y, Oreg Y, Heiblum M and Shtrikman H 2012 *Nat. Phys.* **8** 887

[47] Xu G, Wang W, Zhang X, Du Y, Liu E, Wang S, Wu G, Liu Z and Zhang X X 2014 *Sci. Rep.* **4** 5709

[48] Wang W, Du Y, Xu G, Zhang X, Liu E, Liu Z, Shi Y, Chen J, Wu G and Zhang X 2013 *Sci. Rep.* **3** 2181

[49] Hikami S, Larkin A I and Nagaoka Y 1980 *Prog. Theor. Phys.* **63** 707

[50] Blundell S and Thouless D 2003 *Am. J. Phys* **71** 94

[51] Kittel C 2004 *Introduction to Solid State Physics* (Chichester: John Wiley & Sons) p. 301

[52] Tari A 2003 *The Specific Heat of Matter at Low Temperatures* (London: Imperial College Press) pp. 60–150